ISSN 0915-633X

NATIONAL INSTITUTE FOR FUSION SCIENCE

Kinetic Simulation of Steady States of Ion Temperature Gradient Driven Turbulence with Weak Collisionality

T.-H. Watanabe and H. Sugama

(Received - Nov. 11, 2003)

NIFS-785 Nov. 2003

RESEARCH REPORT
NIFS Series

TOKI, JAPAN

Kinetic simulation of steady states of ion temperature gradient driven turbulence with weak collisionality

T.-H.Watanabe and H.Sugama
National Institute for Fusion Science / The Graduate University for Advanced Studies, Toki, Gifu, 509-5292, Japan
(Dated: November 14, 2003)

Statistically steady states of the ion temperature gradient driven turbulence with weak collisionality are investigated by means of a kinetic simulation based on the gyrokinetic equations. Even if the collision frequency is much lower than characteristic ones of the turbulence, it is indispensable to realizing a steady state of perturbed distribution function δf. In a low-collisionality limit, the low-order velocity-space moments of δf as well as the ion heat transport flux agree with those in the quasisteady state of the collisionless turbulence. A spectral analysis of δf in the velocity-space clarifies the transfer and dissipation processes of the entropy variable associated with fluctuations, where the phase mixing, the $\mathbf{E} \times \mathbf{B}$ nonlinearity, and the finite collisionality are taken into account. A power-law scaling predicted by the theoretical analysis is also verified by the simulations in a subrange of the power spectrum which is free from the entropy production and the collisional dissipation.

Keywords: gyrokinetics, turbulence, transport, computer simulation

PACS numbers: 52.25.Fi, 52.35.Ra, 52.65.-y

I. INTRODUCTION

Turbulent transport in high-temperature plasmas has long been a key issue in the magnetic confinement fusion research [1], since it is considered as a main cause of the anomalous transport of particles and energy. Understanding the microscopic turbulence is important as the first step to prediction and control of the anomalous transport. Extensive simulation studies [2] on drift wave turbulence, such as the ion temperature gradient (ITG) mode, have revealed several important aspects of the turbulent transport in magnetically-confined plasmas, for example, the transport suppression by the self-generated zonal flow [3]. Nevertheless, saturation mechanism of the collisionless turbulence has been an open question. Since the collisionless gyrokinetic equation has the time-reversal symmetry, one needs to consider a coarse-grained form of the one-body velocity distribution function f with small-scale fluctuations in order to define an irreversible transport process in collisionless turbulence.

It has been pointed out that, when a steady transport flux is observed in the collisionless turbulence, a quasisteady state should be realized [4–6], where high-order velocity-space moments of the perturbed distribution function δf continue to grow but the low-order ones are constant in average. Here, $\delta f \equiv f - F_M$ is deviation from the equilibrium given by the Maxwellian velocity distribution F_M. Existence of the quasisteady state in the collisionless ITG turbulence has been confirmed by means of an Eulerian (so-called Vlasov) numerical simulation of the gyrokinetic equation [7]. The phase mixing generates fine-scale fluctuations of δf, and leads to continuous growth of the high-order moments as well as an entropy variable associated with fluctuations (that is defined by a square-integral of δf) of which the growth rate balances with the transport flux multiplied by a normalized ion temperature gradient (see section III A in more detail).

If the collisionless assumption has a practical meaning for considering the steady anomalous transport in an actual plasma with weak but finite collisionality, the quasisteady state should be an idealization of a *real* statistically steady state in a weak-collisionality limit. Namely, for sufficiently low collision frequencies, statistical behaviors of the low-order moments such as the transport flux should agree with those in the collisionless turbulence. Our concern here is, thus, to find the collisionality dependence of the kinetic ITG turbulent transport, and to examine the above conjecture on the relation between the steady and quasisteady states. Introduction of the finite collisionality allows the system to approach the real steady state. Even if the collision frequency is much lower than characteristic ones of the ITG modes, it definitely affects evolution of the system through dissipation of the fine-scale fluctuations of δf in the velocity space.

In simulations of the ITG turbulence shown below, we employ a two-dimensional slab model without complication of interaction between the zonal flow and the turbulence, as has been done in our previous work [7]. The Eulerian kinetic simulation with the simplified model setting enables us not only to investigate fundamental processes in plasma turbulence, such as the $\mathbf{E} \times \mathbf{B}$ advection, the phase mixing and the collisional dissipation, but also to give a useful reference for construction of kinetic-fluid closure models [6, 8]. This is because collisionless fluid simulations of the steady turbulence transport are based on the conjecture on existence of the quasisteady state of turbulence. A detailed comparison between the collisionless kinetic and fluid simulations of the slab ITG turbulence has recently been carried out [9], where the transport coefficient given by the fluid simulation with the nondissipative closure model is in good agreement with the kinetic results.

In the latter part of this paper, a velocity-space power spectrum of δf represented by a quadratic form of the Hermite-polynomial expansion coefficients is investigated in analogy with the passive scalar convection in the homogeneous isotropic turbulence of a neutral fluid [10]. The spectral analysis elucidates the entropy transfer process from macro to micro scales in the phase space through the phase mixing and the $\mathbf{E} \times \mathbf{B}$ nonlinearity. The entropy variable is damped by collisions in a micro velocity scale. Similarly to the viscous-convective subrange in a power spectrum of the passive scalar, we identify a subrange in the power spectrum of δf which is free from the entropy production and the collisional dissipation. A scaling-law for the spectrum of the entropy variable in this subrange will also be derived in this paper.

This paper is organized as follows. Our simulation model is described in Sec. II. Simulation results are presented in Sec. III, where the statistically steady state of the weakly collisional turbulence is discussed in Sec. III A. The collision frequency dependence of the transport flux and a convergence check to mode truncation in the wave number space are given in Secs. III B and C, respectively. The spectral analysis of the distribution function is described in Sec. IV. The obtained results are summarized in Sec. V.

II. SIMULATION MODEL

Our simulation model considered here is the same as in the previous work on the collisionless ITG turbulence except for an ion-ion collision term. We consider a periodic two-dimensional slab configuration with translational symmetry in the z-direction, where the uniform magnetic field is set in the y-z plane such that $\mathbf{B} = B(\hat{z}+\theta\hat{y})$ with $\theta \ll 1$. Equations numerically solved here are derived from a $v_\perp$-integral of the gyrokinetic equations [11] by neglecting the parallel nonlinear term and by assuming $\delta f_{\mathbf{k}}(v_\parallel, v_\perp) = \tilde{f}_{\mathbf{k}}(v_\parallel) F_M(v_\perp)$, where F_M denotes the Maxwellian velocity distribution. We also assume constant density and temperature gradients of the background ions in the x-direction with much larger scale-lengths [$L_n \equiv -d(\ln n)/dx$ and $L_T \equiv -d(\ln T_i)/dx$] than the fluctuation wave lengths. Therefore, we arrive at the following equations represented in the wave number space $\mathbf{k} = (k_x, k_y)$ as

$$\partial_t \tilde{f}_{\mathbf{k}} + i\Theta v_\parallel k_y \tilde{f}_{\mathbf{k}} + \sum_{\mathbf{k}=\mathbf{k}'+\mathbf{k}''} \left(k'_y k''_x - k'_x k''_y\right) \Psi_{\mathbf{k}'} \tilde{f}_{\mathbf{k}''} = -ik_y \Psi_{\mathbf{k}} \left[1 + (v_\parallel^2 - 1 - k^2)\eta_i/2 + \Theta v_\parallel\right] F_M(v_\parallel) + C_i(\tilde{f}_{\mathbf{k}}) \tag{1}$$

and

$$\left[1 - \Gamma_0(k^2)\right] \phi_{\mathbf{k}} = e^{-k^2/2} \int \tilde{f}_{\mathbf{k}}(v_\parallel) dv_\parallel - \tilde{n}_{e,\mathbf{k}} \ , \tag{2}$$

where the electric potential $\phi_{\mathbf{k}}$ is related to $\Psi_{\mathbf{k}}$ by $\Psi_{\mathbf{k}} = e^{-k^2/2}\phi_{\mathbf{k}}$ with $k^2 = k_x^2 + k_y^2$. The background electron temperature $T_e = T_i$ and the adiabatic electron response are also assumed, such that $\tilde{n}_{e,\mathbf{k}} = \phi_{\mathbf{k}}$ for $k_y \neq 0$. Here, for comparison between the collisionless and weakly collisional turbulence, we consider a limiting case with no zonal flow component of $k_y = 0$ by fixing $\tilde{f}_{k_y=0} = \phi_{k_y=0} = 0$, as has been done in our previous simulation [7] with the aim of simulating a large transport level observed in a toroidal geometry. In the slab configuration, otherwise, the turbulence is too severely suppressed by the zonal flow to cause a mean transport [7]. The assumption of no zonal flow also enables us to examine a finite-collisionality effect on turbulence without complication of the collisional damping of the zonal flow and its interplay with turbulence [12]. In addition, we neglect $k_x = 0$ modes of $\tilde{f}_{\mathbf{k}}$ and $\phi_{\mathbf{k}}$, since they are included in the background part with constant density and temperature gradients in the x-direction [13].

Equations (1) and (2) are normalized as follows; $x = x'/\rho_i$, $y = y'/\rho_i$, $v = v'/v_{ti}$, $t = t' v_{ti}/L_n$, $\tilde{f} = \tilde{f}' L_n v_{ti}/\rho_i n_0$, and $\phi = e\phi' L_n/T_i\rho_i$, where v_{ti}, ρ_i ($= v_{ti}/\Omega_i$), Ω_i, n_0, e, and T_i are the ion thermal velocity, the ion thermal gyro-radius, the ion cyclotron frequency, the background plasma density, the elementary charge, and the background ion temperature ($T_i = m_i v_{ti}^2$; m_i means the ion mass), respectively. Prime means a dimensional quantity. Θ is defined as $\Theta = \theta L_n/\rho_i$. η_i and $\Gamma_0(k^2)$ are given by $\eta_i = L_n/L_T$ and $\Gamma_0(k^2) = \exp(-k^2) I_0(k^2)$, respectively. $I_0(z)$ is the 0-th modified Bessel function of z.

The parallel advection term on the left hand side of Eq.(1) contributes to generation of fine-scale fluctuations of $\tilde{f}_{\mathbf{k}}$ in the velocity space, that is, the phase mixing. The instability drive is contained in the first term on the right-hand side of Eq.(1). The second term on the right-hand side denotes the ion-ion collision term for which we employ the Lenard-Bernstein model collision operator,

$$C_i(\tilde{f}_{\mathbf{k}}) = \nu \partial_{v_\parallel} [\partial_{v_\parallel} + v_\parallel] \tilde{f}_{\mathbf{k}}(v_\parallel) \ , \tag{3}$$

with the collision frequency ν normalized by v_{ti}/L_n. The collision operator in Eq.(3) makes $\tilde{f}_{\mathbf{k}}$ approach F_M preserving the mass. Although the momentum and the energy are not conserved, it doesn't cause a significant influence on the results in the present study.

Velocity-space derivatives in the collision term are calculated in the velocity wave number space l into which $\tilde{f}_{\mathbf{k}}(v_\parallel)$ is Fourier-transformed from the $v_\parallel$-space discretized by a uniform grid in a range of $-v_{\max} \leq v_\parallel \leq v_{\max}$ with $v_{\max} = 10 v_{ti}$. Then, they are transformed back to the $v_\parallel$-space. $\tilde{f}_{\mathbf{k}}$ is fixed to zero at $v_\parallel = \pm v_{\max}$, since the fluctuation amplitude at the velocity-space boundary is negligibly small. For the collisionless case, we set $v_{\max} = 5 v_{ti}$. We have employed sufficient resolution of the velocity space in accordance to the magnitude of ν; finer grid spacing for $v_\parallel$ is necessary for a smaller value of ν. Numerical time integration is carried out by the

fourth-order Runge-Kutta-Gill method with careful convergence checks to the time step Δt so as to keep enough accuracy, while a nondissipative time-integration scheme is employed for the collisionless simulation [14, 15]. The minimum and maximum values of the wave number are set to $k_{\min} = 0.1$ and $k_{\max} = 3.2$, respectively, for both of the k_x- and k_y-directions with the 3/2-rule for de-aliasing in the spectral method. Results of a convergence check to $k_{\max}$ are given in Sec. III C.

III. SIMULATION RESULTS

A. Steady state of weakly collisional turbulence

In the system described above, we note a balance equation of entropy variable defined by a functional, $\delta S = \sum_{\mathbf{k}} \int dv_\parallel |\tilde{f}_{\mathbf{k}}|^2/2F_M$, that is,

$$\frac{d}{dt}(\delta S + W) = \eta_i Q_i + D \ , \tag{4}$$

which is derived from Eq.(1) by multiplying $\tilde{f}^*_{\mathbf{k}}/F_M$ (where asterisk denotes complex conjugate) and taking the velocity-space integral and summation over $\mathbf{k}$. Here, Q_i, W, and D are defined as the perpendicular ion heat flux $Q_i = \sum_{\mathbf{k}} \int dv_\parallel (-ik_y e^{-k^2/2}\phi_{\mathbf{k}}) v_\parallel^2 \tilde{f}_{-\mathbf{k}}/2$, the potential energy $W = \sum_{\mathbf{k}} [1 + (T_e/T_i)(1-\Gamma_0)]|\phi_{\mathbf{k}}|^2/2$, and the collisional dissipation $D = \sum_{\mathbf{k}} \int dv_\parallel \tilde{f}_{-\mathbf{k}} C_i(\tilde{f}_{\mathbf{k}})/F_M = -\nu \sum_{\mathbf{k}} \int dv_\parallel |\partial_{v_\parallel} \tilde{f}_{\mathbf{k}} + v_\parallel \tilde{f}_{\mathbf{k}}|^2/F_M < 0$, respectively. It is also remarked that δS is rewritten as $\delta S = S_M - S_m$ within the second order for $\delta f = f - F_M$, where $S_M = -\int d^3v F_M \ln F_M$ and $S_m = -\langle \int d^3v f \ln f \rangle$ represent macroscopic and microscopic entropy per unit volume, respectively. $\langle \cdots \rangle$ means ensemble average. Here, δS corresponds to the opposite sign of the excess entropy defined by Glansdorff and Prigogine [16].

In the collisionless system with $\nu = 0$, as we have shown in Ref.[7] for the no zonal flow case, the quasisteady state characterized by monotonical increase of δS is realized in turbulence while keeping W and Q_i constant in average, that is,

$$\overline{d(\delta S)/dt} \approx \eta_i \overline{Q_i} \ , \tag{5}$$

where $\overline{\cdots}$ indicates time averaging on a certain period longer than a characteristic time of the turbulence. On the other hand, even if ν is much smaller than inverse of the characteristic time of instabilities, introduction of the collision term may lead to statistically steady turbulence, where not only low-order moments but also the distribution function itself are statistically steady. Therefore, in the case with finite collisionality, it is expected that $\overline{d(\delta S)/dt} \approx 0$ and

$$\eta_i \overline{Q_i} \approx -\overline{D} > 0 \ . \tag{6}$$

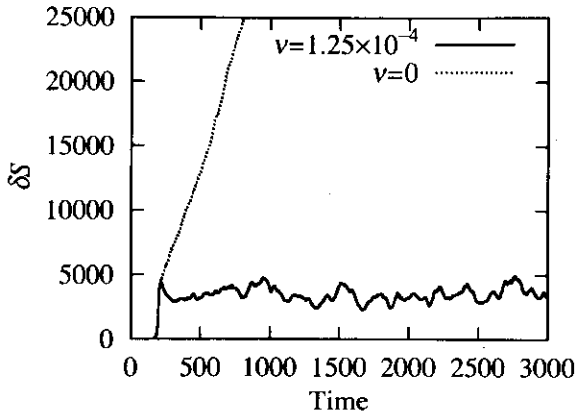

FIG. 1: Time-evolution of δS for collisionless ($\nu = 0$) and weakly collisional ($\nu = 1.25 \times 10^{-4}$) cases.

In order to examine effects of the finite collisionality, we have performed several simulations for different ν's. Throughout the simulation runs shown below, we set $\eta_i = 10$ and $\Theta = 2.5$. For these parameters, in the collisionless case, the angular frequency ω_r and the linear growth rate ω_i of the most unstable mode with $k_x = 0.1$ and $k_y = 0.3$ are $\omega_r = -0.957$ and $\omega_i = 7.73 \times 10^{-2}$, respectively, of which changes due to finite values of ν are negligible in the present parameter range. δS given by the weakly collisional simulation of the ITG turbulence for $\nu = 1.25 \times 10^{-4}$ is plotted as a function of time in Fig.1, where the collisionless simulation result is also shown as a reference. Time-evolutions of δS for different values of ν [which is changed from $(1/512) \times 10^{-3}$ to 8×10^{-3}] are similar to that for $\nu = 1.25 \times 10^{-4}$ in Fig.1. In the quasisteady state of the collisionless turbulence, one finds the monotonical increase of δS, while the potential energy W and the heat flux Q_i are saturated [7]. In the finite collisionality case, however, the growth of δS ceases in the turbulence as well as W and Q_i. It means that not only the low-order but also the high-order moments of δf are statistically steady in the weakly collisional case, since δS is also represented by the sum of squares of the velocity space moments, $\delta S = \sum_n \delta S_n$ [see Eq.(8) for definition of δS_n] [6]. Time-histories of each term in Eq.(4), $d(\delta S)/dt$, dW/dt, $\eta_i Q_i$, and D for $\nu = 1.25 \times 10^{-4}$, are plotted in Fig.2, where data are running-averaged for a time period of $\tau = 50$. One can see that the collisional dissipation D balances with the mean transport, that is, $\eta_i \overline{Q_i} \approx -\overline{D}$, while $\overline{d(\delta S)/dt} \approx \overline{dW/dt} \approx 0$. This also means that the weakly collisional turbulence is in the real statistically steady state. The high accuracy in calculation of the entropy balance is achieved by the sufficient velocity-space resolution of the Eulerian kinetic simulation.

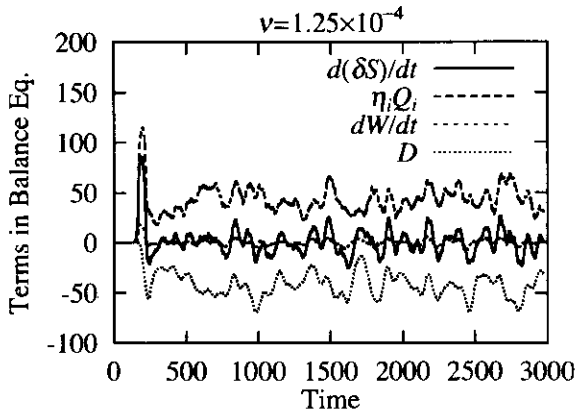

FIG. 2: Time-history of each term in Eq.(4), $d(\delta S)/dt$, dW/dt, $\eta_i Q_i$, and D for $\nu = 1.25 \times 10^{-4}$, where data are running-averaged for a time period of $\tau = 50$.

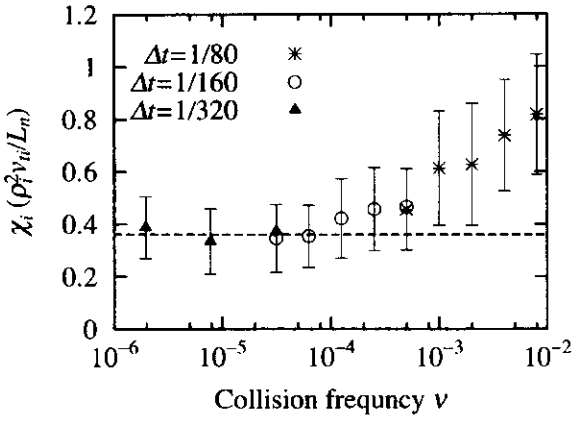

FIG. 3: Anomalous ion heat transport coefficient (χ_i) for different collision frequency ν averaged from $t = 1000$ to 3000. A horizontal dashed line represents χ_i for $\nu = 0$.

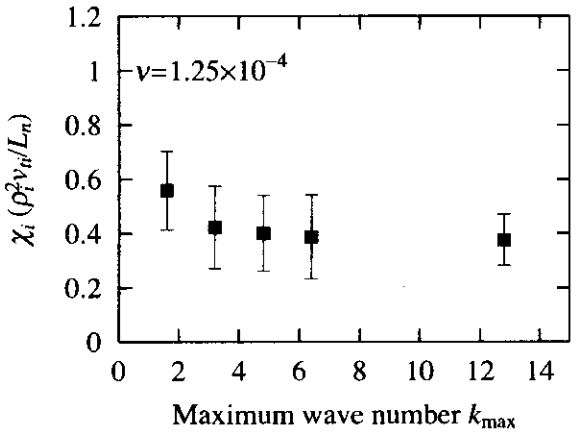

FIG. 4: Ion heat transport coefficient χ_i for different truncation wave numbers $k_{\max}$ with $\nu = 1.25 \times 10^{-4}$.

B. Collision frequency dependence of transport

Collision frequency dependence of the ion heat transport coefficient, $\chi_i \equiv Q_i/\eta_i$, is summarized in Fig.3 where the time-average is taken from $t = 1000$ to 3000. According to the value of ν, the time step Δt is changed from 1/80 to 1/320 so that the numerical error in Eq.(4) should be much smaller than $\eta_i \overline{Q_i}$ and $\overline{D}$. The error bars are estimated from the standard deviation of running-averaged χ_i for a time period $\tau = 10$. In a range of $1.25 \times 10^{-4} < \nu < 8 \times 10^{-3}$, χ_i has a logarithmic dependence on ν. The ν-dependence of χ_i becomes quite weak for lower collision frequencies ($\nu \leq 1.25 \times 10^{-4}$), where χ_i approaches a level of the collisionless one shown by a horizontal dashed line in Fig.3, that is, $\chi_i \approx 0.36 \rho_i^2 v_{ti}/L_n$. From the results shown in Figs.1 to 3, it is summarized that, if ν is small enough, then, the collision term does not influence the low-order moments of δf as well as the transport coefficient χ_i, while it is indispensable to realizing the statistically steady turbulence through damping of the high-order ones generated by the phase mixing. These facts agree with a concept that the quasisteady state is regarded as an idealization of the real steady state in the weak-collisionality limit [6].

C. Convergence check to mode truncation

We have also carried out simulation runs with different values of the maximum wave number $k_{\max}$ in mode truncation such as $k_{\max} = 1.6$, 3.2, 4.8, 6.4, and 12.8, for $\nu = 1.25 \times 10^{-4}$. The results are summarized in Fig.4 in terms of the ion heat transport coefficient χ_i. The numerical simulation is carried out up to $t = 3000$, and the time-averaging period is the same as those in Fig.3. However, the simulation with $k_{\max} = 12.8$ could only be run up to $t = 1200$, because it requires a large amount of computational cost. The time averaging is, thus, taken from $t = 1000$ to 1200, although it doesn't affect the results. One can see good convergence of χ_i for $k_{\max} \geq 3.2$, while χ_i for $k_{\max} = 1.6$ is about 30% larger than the others. One of the reasons is that, in case of $k_{\max} = 1.6$, the potential amplitude at $k = k_{\max}$ is not sufficiently damped by the finite Larmor radius (FLR) effect that is represented as $\exp(-k^2/2)$ in the definitions of $\phi_{\mathbf{k}}$ and $\Psi_{\mathbf{k}}$. Convergence of the simulation results to $k_{\max}$ is also discussed in the next section.

IV. SPECTRAL ANALYSIS OF THE DISTRIBUTION FUNCTION IN THE VELOCITY SPACE

A. Theoretical framework

The parallel advection term in Eq.(1) generates fine-scale fluctuations of the perturbed distribution function

δf in the velocity space (phase mixing). The small-scale components of δf are effectively damped by the collision term with the second derivative in $v_\parallel$. Here, we investigate a power spectrum of the velocity distribution function δf. For the spectral analysis of δf, it is meaningful to pay attention to the transfer of the entropy variable δS from macro to micro velocity scales. Using the basic equations, Eqs.(1) and (2), we obtain

$$\frac{d}{dt}\left[\delta S_n + \delta_{n,1}\frac{1}{2}\sum_{\mathbf{k}}|\phi_{\mathbf{k}}|^2\{1-\Gamma_0(b_{\mathbf{k}})\}\right] = J_{n-1/2} - J_{n+1/2} + \delta_{n,2}\eta_i Q_i - 2\nu n\delta S_n, \quad (7)$$

where

$$\delta S_n \equiv \sum_{\mathbf{k}}\delta S_{\mathbf{k},n} \equiv \sum_{\mathbf{k}}\frac{1}{2}n!|\hat{f}_{\mathbf{k},n}|^2, \quad (8)$$

$$J_{n-1/2} \equiv \sum_{\mathbf{k}}\Theta k_y n!\mathrm{Im}(\hat{f}_{\mathbf{k},n-1}\hat{f}^*_{\mathbf{k},n}), \quad (9)$$

$$J_{n+1/2} \equiv \sum_{\mathbf{k}}\Theta k_y n!\mathrm{Im}(\hat{f}_{\mathbf{k},n}\hat{f}^*_{\mathbf{k},n+1}), \quad (10)$$

and $\delta_{n,m} = 1(n=m), 0(n\neq m)$. Here $\hat{f}_{\mathbf{k},n}$ $(n = 0,1,2,\cdots)$ are defined as coefficients in the Hermite-polynomial expansion of $\tilde{f}_{\mathbf{k}}$,

$$\tilde{f}_{\mathbf{k}}(v_\parallel) = \sum_{n=0}^{\infty}\hat{f}_{\mathbf{k},n}H_n(v_\parallel)F_M(v_\parallel). \quad (11)$$

In the steady state, the left-hand side of Eq.(7) vanishes. We see that $J_{n-1/2}$ ($J_{n+1/2}$) represents the entropy transfer from the $(n-1)$th (nth) to the nth [$(n+1)$th] Hermite-polynomial portion. The third and fourth terms on the right-hand side of Eq.(7) represents the entropy production due to the downward turbulent heat flux in the temperature gradient and the collisional dissipation, respectively. It is important to note that, in the range $n \geq 3$, the entropy production rigorously disappears, which is the reason why the Hermite-polynomial expansion is employed here. A clear cutoff of the entropy production like this never occurs if we use the Fourier expansion in terms of $\exp(ilv_\parallel)$ $(-\infty < l < \infty)$ as basis functions.

Note that

$$H_n(x)e^{-x^2/2} = \frac{i^n}{\sqrt{2\pi}}\int_{-\infty}^{\infty}dl\, e^{ilx}e^{-l^2/2}l^n, \quad (12)$$

where the function $e^{-l^2/2}l^n$ of l has the maximum absolute value at $l = \pm\sqrt{n}$ and is expanded around it as

$$e^{-l^2/2}l^n \simeq e^{-n/2}n^{n/2}[1-(l\mp\sqrt{n})^2]. \quad (13)$$

Thus, the main contribution to the nth component of the Hermite expansion is from the Fourier components with $|l/\sqrt{n}\mp 1| < 1/\sqrt{n}$ so that we may use the relation $n \simeq l^2$ for $n \gg 1$. The inverse of Eq.(12) is given by

$$e^{ilx} = e^{-l^2/2}\sum_{n=0}^{\infty}H_n(x)\frac{i^n l^n}{n!}. \quad (14)$$

The phase mixing process described in Eq.(1) causes the factor $\exp[il(t)v_\parallel]$ in the distribution function, where $l(t)$ satisfies $dl(t)/dt = -\Theta k_y$. Then, the sign of $l(t)$ is opposite to that of k_y for large t so that we write $l(t) \simeq -(k_y/|k_y|)\sqrt{n(t)}$ with the order $n(t)$ of the Hermite-polynomial expansion as a function of t.

For $n \geq 3$ in the steady state, we find from Eq.(7) that

$$-2\nu n\delta S_n = J_{n+1/2} - J_{n-1/2} \simeq \frac{dJ_n}{dn}, \quad (15)$$

where n is treated like a continuous variable and the finite difference is approximated by the derivative. The ratio of J_n to δS_n is written as

$$\frac{J_n}{\delta S_n} = \frac{(n+1/2)!\sum_{\mathbf{k}}\Theta k_y\mathrm{Im}(\hat{f}_{\mathbf{k},n-1/2}\hat{f}^*_{\mathbf{k},n+1/2})}{\frac{1}{2}n!\sum_{\mathbf{k}}|\hat{f}_{\mathbf{k},n}|^2} \simeq 2\Theta\sqrt{n}\frac{\sum_{\mathbf{k}}|k_y||\hat{f}_{\mathbf{k},n}|^2}{\sum_{\mathbf{k}}|\hat{f}_{\mathbf{k},n}|^2} \equiv 2\Theta\sqrt{n}\langle|k_y|\rangle_n, \quad (16)$$

where $(n+1/2)!/n! = \Gamma(n+3/2)/\Gamma(n+1) \simeq \sqrt{n}$ for large n and the averaging operator $\langle\cdot\rangle_n \equiv (\sum_{\mathbf{k}}|\hat{f}_{\mathbf{k},n}|^2\cdot)/(\sum_{\mathbf{k}}|\hat{f}_{\mathbf{k},n}|^2)$ are used. In Eq.(16), we put $\hat{f}_{\mathbf{k},n-1/2}\hat{f}^*_{\mathbf{k},n+1/2} \simeq -i(k_y/|k_y|)|\hat{f}_{\mathbf{k},n}|^2$ by assuming the n-dependence of the phase of $\hat{f}_{\mathbf{k},n}$ to be described mainly by Eq.(14) with $l \simeq -(k_y/|k_y|)\sqrt{n}$.

Now, let us examine the role of $\mathbf{E}\times\mathbf{B}$ convection term. In analogy with the study by Batchelor on the spectrum of the passive scalar for wave lengths smaller than the Kolmogorov scale in the large Prandtl number case [10], we postulate that, for large n, $\hat{f}_{\mathbf{k},n}$ varies so rapidly that $\mathbf{E}\times\mathbf{B}$ flow acting on $\hat{f}_{\mathbf{k},n}$ is regarded as a steady one which is statistically independent of $\hat{f}_{\mathbf{k},n}$. Then, the strain of the steady flow is considered to cause the exponential growth of the wave number of the convected variable. Thus, writing $k_y(t) \propto e^{\gamma t}$ and using $\sqrt{n} = -(k_y/|k_y|)l = \Theta\int dt|k_y|$, we have $\Theta|k_y| \simeq \gamma\sqrt{n}$ which is substituted into Eq.(16) to yield

$$J_n/\delta S_n = 2\gamma n. \quad (17)$$

Substituting Eqs.(17) into (15) and integrating it with respect to n, we obtain

$$\delta S_n = \frac{\sigma}{2\gamma n}\exp\left(-\frac{\nu n}{\gamma}\right), \quad (18)$$

where σ coincides with the entropy production rate as shown by the constraint derived from Eq.(7),

$$\sigma = 2\nu\int_0^{\infty}n\delta S_n dn \simeq 2\nu\sum_n n\delta S_n = \eta_i Q_i. \quad (19)$$

Thus, in the range where neither entropy production nor collisional dissipation occurs ($1 \ll n \ll \gamma/\nu$), we expect the power-law of $\delta S_n \propto 1/n$ with $J_n = \sigma = \text{const.}$ which is analogous to the passive scalar spectrum and its power transfer in the viscous-convective subrange.

In the above analytical treatment, $\langle|k_y|\rangle_n \propto \sqrt{n}$ increases infinitely with n. However, in the numerical simulation performed in the present study, there exists the upper limit of $|\mathbf{k}|$. Even if the potential amplitude is sufficiently damped at the maximum wave number in the simulation, still $f_{\mathbf{k},n}$ for large $|\mathbf{k}|$ and large n is continuously produced by the combination of the $\mathbf{E} \times \mathbf{B}$ convection and the phase mixing process. Therefore, saturation of $\langle|k_y|\rangle_n$ with increasing n is anticipated due to the upper limit of $|\mathbf{k}|$. In this case, taking $\Theta\langle|k_y|\rangle_n = \gamma_M$ as independent of n, we obtain from Eqs.(15) and (16),

$$J_n/\delta S_n = 2\gamma_M\sqrt{n}, \tag{20}$$

and

$$\delta S_n = \frac{\sigma}{2\gamma_M\sqrt{n}} \exp\left(-\frac{2}{3}\frac{\nu n^{3/2}}{\gamma_M}\right), \tag{21}$$

where σ is the same as given by Eq.(19).

B. Application to the simulation results

Let us compare the theoretical analysis given above with the simulation results. For different collision frequencies ν, we have plotted δS_n and $J_{n-1/2}/\sigma$ in Figs.5 and 6, respectively. The maximum wave number is $k_{\max} = 3.2$. One can see that, δS_n at $n = 1$, 2, and 3 has almost the same values for different ν, and is followed by a power-law profile but with ν-dependent exponents [$\delta S_n \propto n^{-\alpha}$ where $\alpha(\nu) > 0$]. Then, δS_n exponentially decays in the dissipation range, where the collision term is dominant, of which a typical value of n is scaled as $n_{\rm d} \propto \nu^{-2/3}$ in consistent with Eq.(21). Thus, $k_{\max}$ affects the spectra for high n's.

Profiles of δS_n obtained by simulations depend on ν as well as $k_{\max}$ and seem to be described by mixture of Eqs.(18) and (21). Certainly, for sufficiently small ν ($\leq 1.25 \times 10^{-4}$), we have confirmed $0.5 < \alpha < 1$. If the collisional dissipation on the left-hand side of Eq.(15) is neglected, one finds that $J_{n-1/2} \simeq$ const. In correspondence, for $\nu \leq 1.25 \times 10^{-4}$, there exists a flat profile of $J_{n-1/2}$ where neither the entropy production nor the collisional dissipation is seen. For larger ν, the subrange with constant $J_{n-1/2}$ ends at relatively small n, which means that the entropy production region on the low n side and the dissipation range are not separated well. Thus, Lower-order moments and transport are influenced by ν. Therefore, it results in the spectrum of δS_n with $\alpha > 1$ for the relatively large values of ν ($\nu > 1.25\times10^{-4}$). It is also noteworthy that the logarithmic dependence of χ_i on ν is observed in Fig.4 for the same parameter range of ν as that discussed here.

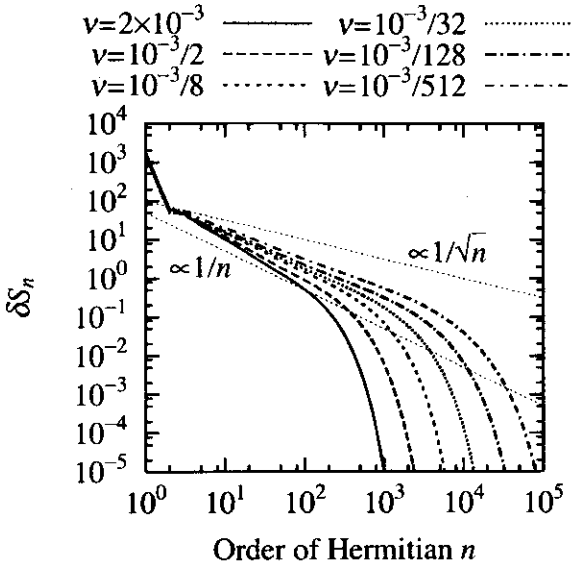

FIG. 5: Spectrum of δS_n versus order of the Hermite-polynomial expansion n for different collision frequencies ν. The maximum wave number is $k_{\max} = 3.2$. Upper and lower dotted straight lines represent $\propto 1/\sqrt{n}$ and $\propto 1/n$, respectively.

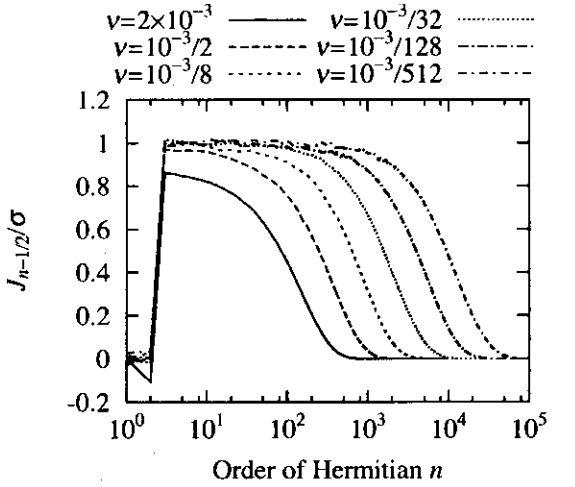

FIG. 6: Plots of $J_{n-1/2}$ defined in Eq.(9) normalized by σ for different collision frequencies ν with $k_{\max} = 3.2$.

The entropy variable $\delta S_{\mathbf{k},n}$ before taking summation over $\mathbf{k}$ in Eq.(7) is transfered in the $(\mathbf{k}, n)$-space by the phase mixing as well as the $\mathbf{E} \times \mathbf{B}$ advection. The latter effect can be found in profiles of $\delta S_{k_y,n} \equiv \sum_{k_x} \delta S_{\mathbf{k},n}$, of which cross-sectional plots are shown in Fig.7 for the case with $\nu = 1.25 \times 10^{-4}$ and $k_{\max} = 12.8$. A steeply-peaked profile of $\delta S_{k_y,n}$ at around $k_y = 0$ in $n < 100$ (as shown by the upper three lines in Fig.7) disappears with increasing n. This is caused by the growth of $\langle|k_y|\rangle$ due to the strain of the $\mathbf{E} \times \mathbf{B}$ flow. Then, the whole profile

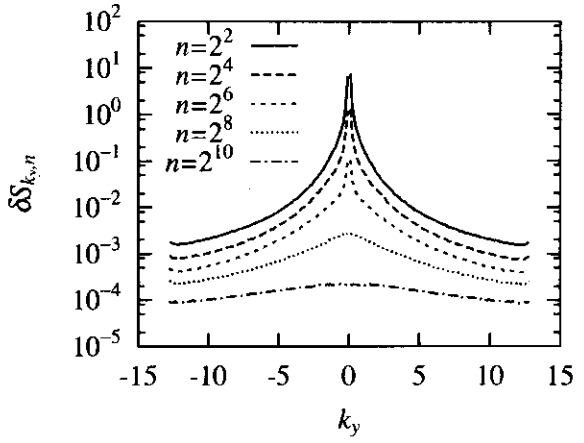

FIG. 7: Cross-sectional plots of $\delta S_{k_y,n}$ versus k_y at $n = 4$, 16, 64, 256, and 1024 for $\nu = 1.25 \times 10^{-4}$ and $k_{\max} = 12.8$.

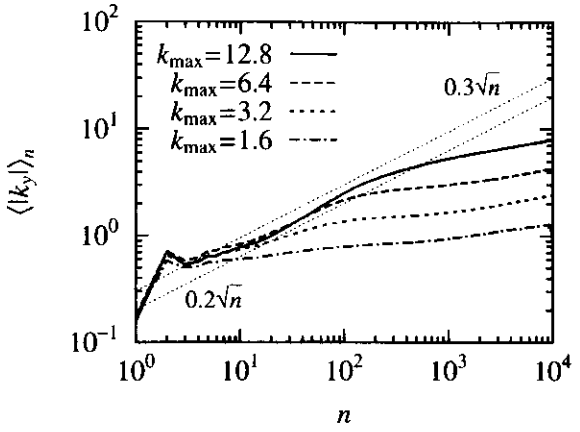

FIG. 8: Spectrum-averaged wave number $\langle|k_y|\rangle$ defined in Eq.(16) for $k_{\max} = 1.6$, 3.2, 6.4, and 12.8 with $\nu = 1.25\times10^{-4}$. Upper and lower dotted lines represent $\langle|k_y|\rangle = 0.3\sqrt{n}$ and $0.2\sqrt{n}$, respectively.

gradually broadens, until the saturation of $\langle|k_y|\rangle$ occurs due to the finite $k_{\max}$.

The growth and saturation of the spectrum-averaged wave number $\langle|k_y|\rangle$ defined in Eq.(16) is more clearly recognized in Fig.8. For $k_{\max} = 12.8$, $\langle|k_y|\rangle$ grows nearly in proportional to $\sqrt{n}$ from $n = 3$ to ~ 100, which agrees with the estimate of $\Theta|k_y| \simeq \gamma\sqrt{n}$ used for derivation of Eq.(17). As n increases, then, the growth of the wave number slows down due to the upper limit $k_{\max}$. A similar evolution of $\langle|k_y|\rangle$ is also found for smaller $k_{\max}$, although the slowdown of the wave number growth is observed at lower n. Even if $k_{\max}$ is small, thus, the values of δS_n at $n = 1$, 2, and 3 are unchanged, except for the case of $k_{\max} = 1.6$ where $\langle|k_y|\rangle$ increases slower than $\sqrt{n}$. The above result is consistent to the convergence check of the transport coefficient χ_i to $k_{\max}$ given in Sec.III C. Therefore, we can conclude that the obtained χ_i as well as the entropy transfer precess on the macro velocity scale but in a small $|\mathbf{k}|$ region is insensitive to the maximum wave number of $k_{\max} \geq 3.2$.

It is meaningful to estimate γ and γ_M from the simulation result. Let us suppose $\langle|k_y|\rangle \sim 0.2\sqrt{n}$ according to Fig.8, and substitute it into $\Theta\langle|k_y|\rangle \simeq \gamma\sqrt{n}$. Thus, we find $\gamma \sim 0.5$ for $\Theta = 2.5$. In the dissipation range of $n \gtrsim 10^3$, however, $\langle|k_y|\rangle \sim 6$ for $k_{\max} = 12.8$ as shown in Fig.8, and thus, $\gamma_M = \Theta\langle|k_y|\rangle \sim 15$. The spectrum δS_n obtained by the simulation with $k_{\max} = 12.8$ is, then, compared with those given by the theoretical analysis with $\sigma = 36$ in Fig.9, where the solid, dashed, and dotted lines indicate the simulation result, Eq.(18) with $\gamma = 0.5$, and Eq.(21) with $\gamma_M = 15$, respectively. One can see that the simulation result is nearly proportional to that of Eq.(18) in a range of $3 \leq n \lesssim 10^3$. In this range $n \lesssim 10^3$, the constant factor $\sigma/2\gamma$ in Eq.(18) gives smaller values of δS_n than that obtained by the simulation. The reason of this is understood as follows. We should recall that the constant factor is derived from the constraint $2\nu \int n\delta S_n dn = \sigma$ where σ is evaluated from

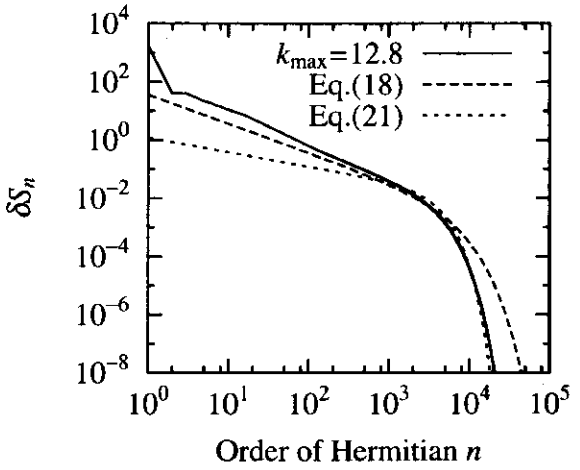

FIG. 9: Plot of δS_n for $\nu = 1.25 \times 10^{-4}$ and $k_{\max} = 12.8$ (solid). Theoretical spectra given by Eq.(18) with $\gamma = 0.5$ and Eq.(21) with $\gamma_M = 15$ are also shown by dashed and dotted lines, respectively, where $\sigma = 36$.

the simulation result. Then, in the range $n \lesssim 10^3$, the spectrum δS_n in Eq.(18) needs to be smaller than that in the simulation in order to satisfy the constraint because, for $n \gtrsim 10^3$, the latter spectrum is smaller than the former due to the effect of finite $k_{\max}$. However, in the dissipation range of $n \gtrsim 10^3$, the spectrum found in the simulation is well fitted by Eq.(21). The above results show that the transfer process of the entropy variable observed by the Eulerian kinetic simulations of the slab ITG turbulence can be well described by combining the analytical expressions in Eqs.(18) and (21) in Sec. IV A. It is expected that, if we can employ an sufficiently high value of $k_{\max}$, the simulation will reproduce the spectrum δS_n in Eq.(18) for the whole range $n \geq 3$.

V. CONCLUDING REMARKS

We have carried out Eulerian kinetic simulations of the slab ITG turbulence with weak collisionality, where we have employed the gyrokinetic equation (integrated for $v_\perp$) with the Lenard-Bernstein model collision operator and the quasi-neutrality condition. Introduction of finite collisionality enables us to find the real statistically steady state of turbulence, where not only the turbulence energy and the transport flux but also the entropy variable $\delta S \equiv \int \delta f^2/2F_M dv$ are constant in average. Then, the ion heat transport flux Q_i multiplied by η_i is balanced with the collisional dissipation. It is contrast to the quasisteady state of the collisionless turbulence, where $d(\delta S)/dt$ balances with $\eta_i Q_i$ but with constant energy [7]. A parameter survey for the collision frequency ν shows the logarithmic dependence of χ_i on relatively large values of ν. For sufficiently low collision frequency, however, the transport coefficient χ_i approaches a value in the collisionless case, which means that the low-order velocity-space moments of the distribution function in the quasisteady state of the collisionless turbulence agree with those in the real steady state of weakly collisional one. It is also confirmed that χ_i has a good convergence to the maximum wave number $k_{\max} \geq 3.2$ employed in the simulations.

We have also made the spectral analysis of the distribution function in the velocity space by means of the Hermite-polynomial expansion with the Maxwellian weight function. The entropy variable δS_n defined by a power spectrum of the distribution function has almost the same values at $n = 1$, 2, and 3 even for different values of ν, where n denotes the order of the Hermite-polynomial expansion. This is consistent with the ν-dependence of χ_i for the low collisionality case described above as well as the conjecture by Krommes and Hu such as '*flux determines dissipation*' [4]. The entropy variable produced on the low n side is transfered in the $(\mathbf{k}, n)$-space by the phase mixing and the $\mathbf{E} \times \mathbf{B}$ nonlinearity. Then, it is dissipated by the collision term on a high n side. Our theoretical analysis of the spectrum well describes how δS_n ($n \gg 3$) depends on n, ν, and $k_{\max}$. In analogy with the passive scalar convection for wave length smaller than the Kolmogorov scale in the large Prandtl number case, the scaling-law, $\delta S_n \propto 1/n$, is found in the subrange of the n-space where neither entropy production nor collisional dissipation occurs.

Acknowledgments

Part of this work was completed when one of the authors (T.-H.W.) was an exchange scientist at the Institute for Fusion Studies, the University of Texas at Austin, under the Joint Institute for Fusion Theory, U.S.-Japan Fusion Cooperation Program. This work is partially supported by grants-in-aid of Ministry of Education, Culture, Sports, Science and Technology (No.12680497 and 14780387).

[1] W. Horton, Rev. Mod. Phys. **71**, 735 (1999).
[2] A. M. Dimits, G.Bateman, M. A. Beer, *et al.*, Phys. Plasmas **7**, 969 (2000).
[3] P. W. Terry, Rev. Mod. Phys. **72**, 109 (2000).
[4] J. A. Krommes and G. Hu, Phys. Plasmas **1**, 3211 (1994).
[5] H. Sugama, M. Okamoto, W. Horton, and M. Wakatani, Phys. Plasmas **3**, 2379 (1996).
[6] H. Sugama, T.-H. Watanabe, and W. Horton, Phys. Plasmas **8**, 2617 (2001).
[7] T.-H. Watanabe and H. Sugama, Phys. Plasmas **9**, 3659 (2002).
[8] G. W. Hammett and F. W. Perkins, Phys. Rev. Lett. **64**, 3019 (1990).
[9] H. Sugama, T.-H. Watanabe, and W. Horton, Phys. Plasmas **10**, 726 (2003).
[10] G. K. Batchelor, J.Fluid Mech. **5**, 113 (1959).
[11] D. H. E. Dubin, J. A. Krommes, C. Oberman, and W. W. Lee, Phys. Fluids **26**, 3524 (1983).
[12] Z. Lin, T. S. Hahm, W. W. Lee, W. M. Tang, and P. H. Diamond, Phys. Rev. Lett. **83**, 3645 (1999).
[13] W. W. Lee, J. Comput. Phys. **72**, 243 (1987).
[14] T.-H. Watanabe, H. Sugama, and T. Sato, Phys. Plasmas **7**, 984 (2000).
[15] T.-H. Watanabe, H. Sugama, and T. Sato, J. Phys. Soc. Jpn. **70**, 3565 (2001).
[16] P. Glansdorff, and I. Prigogine, "*Thermodynamic Theory of Structure, Stability and Fluctuations*" (Wiley-Interscience, London, 1971).

Recent Issues of NIFS Series

NIFS-762 S. Okamura, K. Matsuoka, S. Nishimura, M. Isobe, C. Suzuki, A. Shimizu, K. Ida, A. Fujisawa, S. Murakami, M. Yokoyama, K. Itoh, T. Hayashi, N. Nakajima, H. Sugama, M. Wakatani, Y. Nakamura, W. Anthony Cooper
Physics Design of Quasi-Axisymmetric Stellarator CHS-qa
Oct. 2002 (IC/P-07)

NIFS-763 Lj. Nikolic, M.M. Skoric, S. Ishiguro and T. Sato
On Stimulated Scattering of Laser Light in Inertial Fusion Energy Targets
Nov. 2002

NIFS-764
NIFS Contributions to 19th IAEA Fusion Energy Conference (Lyon, France, 14-19 October 2002)
Nov. 2002

NIFS-765 S. Goto and S. Kida
Enhanced Stretching of Material Lines by Antiparallel Vortex Pairs in Turbulence
Dec. 2002

NIFS-766 M. Okamoto, A.A. Maluckov, S. Satake, N. Nakajima and H. Sugama
Transport and Radial Electric Field in Torus Plasmas
Dec. 2002

NIFS-767 R. Kanno, N. Nakajima, M. Okamoto and T. Hayashi
Computational Study of Three Dimensional MHD Equilibrium with m/n=1/1 Island
Dec. 2002

NIFS-768 M. Yagi, S.-I. Itoh, M. Kawasaki, K. Itoh and A. Fukuyama
Multiple-Scale Turbulence and Bifurcaion
Jan. 2003

NIFS-769 S.-I. Itoh, K. Itoh and S. Toda
Statistical Theory of L-H Transition and its Implication to Threshold Database
Jan. 2003

NIFS-770 K. Itoh
Summary: Theory of Magnetic Confinement
Jan. 2003

NIFS-771 S.-I. Itoh, K. Itoh and S. Toda
Statistical Theory of L-H Transition in Tokamaks
Jan. 2003

NIFS-772 M. Stepic, L. Hadzievski and M.M. Skoric
Modulation Instability in Two-dimensional Nonlinear Schrodinger Lattice Models with Dispersion and Long-range Interactions
Jan. 2003

NIFS-773 M.Yu. Isaev, K.Y. Watanabe, M. Yokoyama and K. Yamazaki
The Effect of Hexapole and Vertical Fields on α-particle Confinement in Heliotron Configurations
Mar. 2003

NIFS-774 K. Itoh, S.-I. Itoh, F. Spineanu, M.O. Vlad and M. Kawasaki
On Transition in Plasma Turbulence with Multiple Scale Lengths
May 2003

NIFS-775 M. Vlad, F. Spineanu, K. Itoh, S.-I. Itoh
Intermittent and Global Transitions in Plasma Turbulence
July 2003

NIFS-776 Y. Kondoh, M. Kondo, K. Shimoda, T. Takahashi and K. Osuga
Innovative Direct Energy Conversion Systems from Fusion Output Thermal Power to the Electrical One with the Use of Electronic Adiabatic Processes of Electron Fluid in Solid Conductors.
July 2003

NIFS-777 S.-I. Itoh, K. Itoh and M. Yagi
A Novel Turbulence Trigger for Neoclassical Tearing Modes in Tokamaks
July 2003

NIFS-778 T. Utsumi, J. Koga, T. Yabe, Y. Ogata, E. Matsunaga, T. Aoki and M. Sekine
Basis Set Approach in the Constrained Interpolation Profile Method
July 2003

NIFS-779 Oleg I. Tolstikhin and C. Namba
CTBC A Program to Solve the Collinear Three-Body Coulomb Problem: Bound States and Scattering Below the Three-Body Disintegration Threshold
Aug. 2003

NIFS-780
Contributions to 30th European Physical Society Conference
on Controlled Fusion and Plasma Physics
(St.Petersburg, Russia, 7-11 July 2003)
from NIFS
Aug. 2003

NIFS-781 Ya. I. Kolesnichenko, K. Yamazaki, S. Yamamoto, V.V. Lutsenko, N. Nakajima, Y. Narushima, K. Toi, Yu. V. Yakovenko
Interplay of Energetic Ions and Alfvén Modes in Helical Plasmas
Aug. 2003

NIFS-782 S.-I. Itoh, K. Itoh and M. Yagi
Turbulence Trigger for Neoclassical Tearing Modes in Tokamaks
Sep. 2003

NIFS-783 F. Spineanu, M. Vlad, K. Itoh, H. Sanuki and S.-I. Itoh
Pole Dynamics for the Flierl-Petviashvili Equation and Zonal Flow
Sep. 2003

NIFS-784 R. Smirnov, Y. Tomita, T. Takizuka, A. Takayama, Yu. Chutov
Particle Simulation Study of Dust Particle Dynamics in Sheaths
Oct. 2003

NIFS-785 T.-H. Watanabe and H. Sugama
Kinetic Simulation of Steady States of Ion Temperature Gradient Driven Turbulence with Weak Collisionality
Nov. 2003